Single-crystal Data of Ternary Germanides $RE_2Nb_3Ge_4$ (RE = Sc, Y, Gd–Er, Lu) and $Sc_2Ta_3Ge_4$ with Ordered Sm_5Ge_4-type Structure

Bastian Reker[a], Samir F. Matar[b], Ute Ch. Rodewald[a], Rolf-Dieter Hoffmann[a], and Rainer Pöttgen[a]

[a] Institut für Anorganische und Analytische Chemie, Universität Münster, Corrensstraße 30, 48149 Münster, Germany

[b] CNRS, Université de Bordeaux, ICMCB, 87 Avenue Dr. A. Schweitzer, 33608 Pessac-Cedex, France

Reprint requests to R. Pöttgen. E-mail: pottgen@uni-muenster.de

Z. Naturforsch. **2013**, *68b*, 625 – 634 / DOI: 10.5560/ZNB.2013-3041
Received February 12, 2013

Dedicated to Professor Heinrich Nöth on the occasion of his 85th birthday

Small single crystals of the Sm_5Ge_4-type (space group *Pnma*) germanides $RE_2Nb_3Ge_4$ (RE = Sc, Y, Gd–Er, Lu) and $Sc_2Ta_3Ge_4$ were synthesized by arc-melting of the respective elements. The samples were characterized by powder and single-crystal X-ray diffraction. In all structures, except for $Sc_{2.04}Nb_{2.96}Ge_4$ and $Sc_{2.19}Ta_{2.81}Ge_4$, the rare earth and niobium atoms show full ordering on the three crystallographically independent samarium sites of the Sm_5Ge_4 type. Two sites with coordination number 6 are occupied by niobium, while the slightly larger site with coordination number 7 is filled with the rare earth element. Small homogeneity ranges with RE/Nb and RE/Ta mixing can be expected for all compounds. The ordered substitution of two rare earth sites by niobium or tantalum has drastic effects on the coordination number and chemical bonding. This was studied for the pair Y_5Ge_4/$Y_2Nb_3Ge_4$. Electronic structure calculations show larger charge transfer from yttrium to germanium for Y_5Ge_4, contrary to $Y_2Nb_3Ge_4$ which shows stronger covalent bonding due to the presence of Nb replacing Y at two sites.

Key words: Rare Earth Compounds, Crystal Structure, Chemical Bonding, Germanium

Introduction

Rare earth-based intermetallic compounds with orthorhombic Sm_5Ge_4-type structure have attracted considerable interest among solid state physicists and chemists, when the giant magnetocaloric effect was discovered in $Gd_5Si_2Ge_2$ [1 – 7, and refs. therein]. These materials have intensively been investigated with respect to solid solutions on both the rare earth and the *p*-element sites in order to improve the magnetocaloric properties. Depending on composition and temperature, samples of these solid solutions show substantial structural distortions.

The Sm_5Ge_4 structure [8, 9] has three crystallographically independent samarium sites, 8*d* (2×) and 4*c*, with different coordination numbers (CN). The 4*c* and one of the 8*d* sites have distorted octahedral germanium coordination (CN 6) while the other 8*d* site has CN 7 in slightly distorted pentagonal bipyramidal coordination. These different coordination motifs imply that an ordered substitution with larger and smaller atoms should be possible. This was first realized for $Ce_2Sc_3Si_4$ [10, 11] and later for a series of compounds with an ordering of larger and smaller (mainly scandium) rare earth atoms [12 – 21]. Isotypic compounds are also formed with the electron-poor transition metals Ti [22 – 24], Nb and Ta [25 – 31], as well as Mo and W [32 – 38]. Most of these compounds were characterized only on the basis of powder X-ray diffraction. In many cases, even long annealing sequences did not yield sufficiently large crystals. Some of these ordered compounds exhibit interesting magnetic properties. $U_2Nb_3Ge_4$ and $U_2Ta_3Ge_4$ are ferromagnets with comparatively high Curie temperatures of 130 and 105 K, respectively [27], while $Tb_2Nb_3Si_4$ and $Ho_2Nb_3Ge_4$ are ordered antiferromagnetically at much lower Néel temperatures of 19 and 25 K [28].

Well-shaped single crystals of the $RE_2Nb_3Ge_4$ germanides have been obtained in our group during synthesis attempts for $RE_4Zn_5Ge_6$ and $RE_5Zn_{4-x}Ge_6$ samples [39] through drastic attack of the niobium ampoules. Subsequently we obtained suitable single crystals of these compounds from a targeted synthesis through repeated arc-melting sequences. The crystal chemical details of these germanides are reported herein.

Experimental

Synthesis

Starting materials for the synthesis of the germanides $RE_2Nb_3Ge_4$ (RE = Sc, Y, Gd, Tb, Dy, Ho, Er) and $Sc_2Ta_3Ge_4$ were ingots of the rare earth metals (Johnson Matthey and smart elements), niobium and tantalum powder (Strem Chemicals) and lumps of germanium (Wacker), all with a stated purity better than 99.9 %. The rare earth metal pieces, the germanium lumps and the niobium (tantalum) powder were weighed in the 2 : 3 : 4 atomic ratios. The germanium lumps were first ground to a fine powder, mixed with the niobium (tantalum) powder and pressed to a pellet. Then the rare earth metal pieces and the pellets were arc-melted in a water cooled copper crucible [40] under an argon atmosphere of about 700 mbar. The argon was purified over titanium sponge (900 K), silica gel, and molecular sieves. The resulting pellet was re-melted several times from each side to ensure homogeneity. Subsequently the product pellets were ground to a homogeneous powder, pressed again to pellets and arc-welded from each side.

Crystals of columnar shape grew on the surface of the product buttons. They could easily be separated mechanically from the carefully crushed buttons. No reaction with the crucible material could be detected. The silvery polycrystalline samples are stable in air over months.

EDX data

Polished micro-sections of each sample as well as the measured crystals were analyzed using a Zeiss EVO MA10 scanning electron microscope with Y, Nb, Ta, Ge, and the rare earth trifluorides as standards. No impurity elements heavier than sodium (detection limit of the instrument) were observed. Both the polished micro-sections and the crystals showed nearly identical compositions which were in good agreement with the ideal ones.

X-Ray diffraction

The polycrystalline samples were characterized by Guinier patterns (imaging plate detector, Fujifilm BAS-1800) with Cu$K_{\alpha1}$ radiation and α-quartz (a = 491.30, c = 540.45 pm) as an internal standard. Correct indexing of the patterns was ensured through intensity calculations [41] using the single crystal data. The orthorhombic lattice parameters (Table 1) were refined by least-squares calculations.

Single crystals of high quality with a columnar shape were selected from the carefully crushed symples. For quality control every crystal was first checked by Laue photographs on a Buerger camera with white Mo radiation. The intensity data sets were collected at room temperature using a Stoe IPDS-II imaging plate diffractometer in oscillation mode (graphite-monochromatized MoK_α radiation) and a Stoe StadiVari equipped with a Mo microfocus source and a Pilatus 100 K Detector with a hybrid-pixel sensor. Numerical absorption corrections were applied to all data sets. Details about the data collections and the crystallographic parameters are summarized in Tables 2 and 3.

Structure refinements

The data sets of the nine crystals showed primitive orthorhombic lattices, and the systematic extinctions were compatible with space group *Pnma*. The standardized atomic parameters of $Ce_2Sc_3Si_4$ [10] were taken as starting values and the structures were refined with the JANA2006 package [42, 43] or SHELXL-97 [44, 45] with anisotropic atomic displacement parameters for all atoms. The data sets of the scandium compounds showed small deviations from the ideal composition, a consequence of Sc/Nb respectively Sc/Ta mixing on the three crystallographically independent samarium sites of the Sm_5Ge_4 type [9]. The mixed occupancies were refined as least-squares variables in the final cycles, leading to the compositions listed in Tables 2 and 3 for the investigated crystals. The final difference Fourier syntheses revealed no significant residual peaks. The refined atomic positions, displacement parameters, and interatomic distances (exemplarily for $Gd_2Nb_3Ge_4$) are given in Tables 4 and 5.

Further details of the crystal structure investigation may be obtained from Fachinformationszentrum Karlsruhe, 76344 Eggenstein-Leopoldshafen, Germany (fax: +49-7247-808-666; e-mail: crysdata@fiz-karlsruhe.de, http://www.fiz-karlsruhe.de/request_for_deposited_data.html) on quoting the deposition numbers CSD-425795 ($Sc_{2.04}Nb_{2.96}Ge_4$), CSD-425790 ($Y_2Nb_3Ge_4$), CSD-425794 ($Gd_2Nb_3Ge_4$), CSD-425793 ($Tb_2Nb_3Ge_4$), CSD-425792 ($Dy_2Nb_3Ge_4$), CSD-425789 ($Ho_2Nb_3Ge_4$), CSD-425791 ($Er_2Nb_3Ge_4$), CSD-425788 ($Lu_2Nb_3Ge_4$), and CSD-425796 ($Sc_{2.19}Ta_{2.81}Ge_4$).

Computational details

For the investigations of the electronic structures and the properties of bonding we considered binary Y_5Ge_4 [6] and $Y_2Nb_3Ge_4$ as representative of the title compounds. The input parameters are those of the experimental crystal structure parameters.

Table 1. Lattice parameters of the ternary germanides $RE_2Ta_3Ge_4$ and $RE_2Nb_3Ge_4$.

Compound	a (pm)	b (pm)	c (pm)	V (nm^3)	Reference
$Sc_2Ta_3Ge_4$	681.61(7)	1323.0(1)	697.27(8)	0.6288	this work
$Sc_2Ta_3Ge_4$	682.3(7)	1318(1)	697.7(7)	0.6274	[37]
$U_2Ta_3Ge_4$	701.5(2)	1345.4(3)	713.9(2)	0.6738	[27]
$Sc_2Nb_3Ge_4$	686.0(7)	1339(1)	716.0(8)	0.6577	[25]
$Sc_2Nb_3Ge_4$	681.9(1)	1325.6(1)	699.0(1)	0.6318	this work
$Y_2Nb_3Ge_4$	696.4(8)	1357.2(13)	718.2(4)	0.6788	[28]
$Y_2Nb_3Ge_4$	701.13(6)	1355.1(1)	717.46(5)	0.6817	this work
$Zr_2Nb_3Ge_4$	686.1(3)	1336.3(4)	700.3(2)	0.6421	[33]
$Gd_2Nb_3Ge_4$	699.8(2)	1355.2(5)	718.4(3)	0.6813	[28]
$Gd_2Nb_3Ge_4$	700.98(8)	1353.6(1)	717.87(8)	0.6811	this work
$Tb_2Nb_3Ge_4$	698.1(4)	1351.5(6)	715.6(6)	0.6752	[28]
$Tb_2Nb_3Ge_4$	698.75(7)	1353.1(1)	716.49(8)	0.6774	this work
$Dy_2Nb_3Ge_4$	697.5(4)	1351.0(11)	715.4(4)	0.6741	[28]
$Dy_2Nb_3Ge_4$	697.49(9)	1349.8(2)	714.8(1)	0.6730	this work
$Ho_2Nb_3Ge_4$	695.6(3)	1347.9(4)	713.1(4)	0.6686	[28]
$Ho_2Nb_3Ge_4$	696.18(6)	1348.9(1)	713.42(8)	0.6700	this work
$Er_2Nb_3Ge_4$	692.7(4)	1346.5(7)	711.6(5)	0.6637	[28]
$Er_2Nb_3Ge_4$	693.81(5)	1345.20(7)	711.21(3)	0.6638	this work
$Tm_2Nb_3Ge_4$	691.7(4)	1341.6(4)	709.2(4)	0.6581	[28]
$Yb_2Nb_3Ge_4$	693.7(1)	1344.9(4)	710.9(2)	0.6632	[28]
$Lu_2Nb_3Ge_4$	689.5(3)	1339.2(5)	707.1(4)	0.6529	[28]
$Lu_2Nb_3Ge_4$	690.7(1)	1339.1(1)	708.2(1)	0.6550	this work
$Hf_2Nb_3Ge_4$	686.3(4)	1336.1(5)	700.6(4)	0.6424	[26]
$U_2Nb_3Ge_4$	701.78(6)	1347.3(2)	715.00(7)	0.6760	[27]

Table 2. Crystal data and structure refinements for $Sc_{2.04}Nb_{2.96}Ge_4$, $Y_2Nb_3Ge_4$, $Gd_2Nb_3Ge_4$, and $Tb_2Nb_3Ge_4$, structure type $Ce_2Sc_3Si_4$, space group *Pnma*, $Z = 4$, Pearson symbol oP36. Note the different sigma cut-offs of $n = 2$ for the SHELXL and $n = 3$ for the JANA calculations.

Empirical formula	$Sc_{2.04}Nb_{2.96}Ge_4$	$Y_2Nb_3Ge_4$	$Gd_2Nb_3Ge_4$	$Tb_2Nb_3Ge_4$
Formula weight, g mol^{-1}	659.0	746.91	883.6	886.9
Unit cell dimensions (Guinier powder data)				
a, pm	681.9(1)	701.13(6)	700.98(8)	698.75(7)
b, pm	1325.6(1)	1355.1(1)	1353.6(1)	1353.1(1)
c, pm	699.0(1)	717.46(5)	717.87(8)	716.49(8)
Cell volume V, nm^3	0.6318	0.6817	0.6811	0.6774
Calculated density, g cm^{-3}	6.93	7.28	8.61	8.69
Crystal size, μm^3	$20 \times 20 \times 120$	$10 \times 20 \times 40$	$20 \times 20 \times 60$	$15 \times 20 \times 90$
Transmission ratio (max / min)	0.74 / 0.42	0.75 / 0.34	0.77 / 0.18	0.62 / 0.18
Diffractometer	IPDS-II	IPDS-II	IPDS-II	IPDS-II
Detector distance, mm	80	60	60	80
Exposure time, min	5	40	6	6
ω range; increment, deg	0–180; 1.0	0–180; 1.0	0–180; 1.0	0–180; 1.0
Integr. param. A; B; EMS	12.8; 2.2; 0.012	12.8; 2.5; 0.012	12.9; 3.1; 0.012	12.6; –4.2; 0.012
Absorption coefficient, mm^{-1}	25.8	38.9	41.5	42.8
F(000), e	1169	1316	1516	1524
θ range for data collection, deg	3.1–31.9	3.0–35.0	3.0–35.1	3.0–32.0
Range in hkl	±10, ±19, ±10	±11, ±21, ±11	±11, ±21, ±11	±10, ±20, ±10
Program system	JANA	SHELXL	JANA	JANA
Total no. of reflections	7347	8294	8734	7151
Independent reflections / R_{int}	1124 / 0.0288	1541 / 0.1725	1541 / 0.0405	1207 / 0.0346
Reflections with $I > n\sigma(I)/R_\sigma$	844 / 0.0244	416 / 0.3717	1029 / 0.0397	895 / 0.0216
Data / ref. parameters	1124 / 49	1541 / 46	1541 / 47	1207 / 47
Goodness-of-fit on F^2	0.53	0.51	1.01	1.27
R / wR for $I > n\sigma(I)$	0.0096 / 0.0094	0.0418 / 0.0892	0.0218 / 0.0225	0.0207 / 0.0240
R / wR for for all data	0.0184 / 0.0103	0.1788 / 0.1095	0.0437 / 0.0242	0.0293 / 0.0243
Extinction coefficient	83(8)	–	115(9)	133(13)
Largest diff. peak / hole, e Å^{-3}	0.66 / –0.86	1.83 / –1.52	3.02 / –2.40	1.39 / –1.31

Table 3. Crystal data and structure refinements for $Dy_2Nb_3Ge_4$, $Ho_2Nb_3Ge_4$, $Er_2Nb_3Ge_4$, $Lu_2Nb_3Ge_4$ and $Sc_{2.19}Ta_{2.81}Ge_4$, structure type $Ce_2Sc_3Si_4$, space group *Pnma*, $Z = 4$, Pearson symbol oP36. Note the different sigma cut-offs of $n = 2$ for the SHELXL and $n = 3$ for the JANA calculations.

Empirical formula	$Dy_2Nb_3Ge_4$	$Ho_2Nb_3Ge_4$	$Er_2Nb_3Ge_4$	$Lu_2Nb_3Ge_4$	$Sc_{2.19}Ta_{2.81}Ge_4$
Formula weight, g mol^{-1}	894.1	898.95	903.6	919.03	923.1
Unit cell dimensions (Guinier powder data)					
a, pm	697.49(9)	696.18(6)	693.81(3)	690.7(1)	681.61(7)
b, pm	1349.8(2)	1348.9(1)	1345.20(7)	1339.1(1)	1323.0(1)
c, pm	714.8(1)	713.42(8)	711.21(3)	708.2(1)	697.27(8)
Cell volume V, nm^3	0.6730	0.6670	0.6638	0.6550	0.6288
Calculated density, g cm^{-3}	8.82	8.91	9.04	9.32	9.75
Crystal size, μm^3	$20 \times 20 \times 100$	$20 \times 50 \times 120$	$20 \times 30 \times 80$	$20 \times 40 \times 50$	$20 \times 30 \times 50$
Transmission ratio (max / min)	0.47 / 0.08	0.41 / 0.11	0.57 / 0.13	0.68 / 0.31	0.38 / 0.13
Diffractometer	StadiVari	IPDS-II	IPDS-II	IPDS-II	StadiVari
Detector distance, mm	80	70	80	80	60
Exposure time, s	35	600	480	300	14
ω range; increment, deg	–; 0.2	0–180; 1.0	0–180; 1.0	0–180; 1.0	–; 0.3
Integr. Param. A; B; EMS	9.6; –7.8; 0.012	13.1; 2.8; 0.012	13.0; 2.8; 0.012	14.0; 2.0; 0.03	8.3; –6.5; 0.013
Absorption coefficient, mm^{-1}	44.3	45.8	48.2	52.8	72.8
F(000), e	1532	1540	1548	1572	1517
θ range for data collection, deg	4.4–33.8	3.0–34.8	3.0–32.0	3.0–32.0	3.1–32.6
Program system	JANA	SHELXL	JANA	SHELXL	JANA
Range in hkl	±10, ±21, ±11	±11, ±21, ±11	±10, ±19, ±10	±10, ±19, ±10	±9, ±19, ±10
Total no. of reflections	8959	8747	7112	7952	7964
Independent reflections / R_{int}	1381 / 0.0269	1499 / 0.0584	1181 / 0.0410	1186 / 0.0639	1146 / 0.0429
Reflections with $I > n\sigma(I)$ / R_σ	1126 / 0.0149	1334 / 0.0317	926 / 0.0187	838 / 0.0700	673 / 0.0813
Data / ref. parameters	1381 / 47	1499 / 47	1181 / 47	1186 / 47	1140 / 49
Goodness-of-fit on F^2	0.99	0.97	1.65	0.88	0.32
R / wR for $I > n\sigma(I)$	0.0134 / 0.0165	0.0276 / 0.0657	0.0224 / 0.0295	0.0349 / 0.0437	0.0112 / 0.0112
R / wR for for all data	0.0193 / 0.0172	0.0329 / 0.0677	0.0320 / 0.0302	0.0728 / 0.0501	0.0258 / 0.0122
Extinction coefficient	136(9)	0.0020(2)	108(15)	0.0004(1)	38(3)
Largest diff. peak / hole, e Å^{-3}	1.21 / –1.05	3.17 / –3.23	2.24 / –2.28	2.36 / –2.28	0.17 / –0.18

All-electron calculations were carried out for a full description of the atom-resolved electronic structures and the properties of chemical bonding. They were performed using the full-potential scalar-relativistic augmented spherical wave (ASW) method [46, 47] built within the well-established quantum theoretical framework of the density functional theory (DFT) [48, 49] with the generalized gradient approximation (GGA) functional for the effects of exchange and correlation following the scheme of Perdew *et al.* [50]. In the ASW method, the wave function is expanded in atom-centered augmented spherical waves, which are Hankel functions and numerical solutions of Schrödinger's equation, respectively, outside and inside the so-called augmentation spheres. In the minimal ASW basis set, we chose the outermost shells to represent the valence states, and the matrix elements were constructed using partial waves up to $l_{max} + 1 = 3$ for Y and Nb and $l_{max} + 1 = 2$ for Ge. For the latter, at low energy lying filled $3d^{10}$ states were considered as core states, *i. e.* not considered in the valence basis set. Self-consistency was achieved when charge transfers and energy changes between two successive cycles were below 10^{-8} and 10^{-6} eV, respectively. The Brillouin zone integrations were performed using the linear tetrahedron method within the irreducible wedge [47]. The calculations were carried out assuming spin degenerate configuration.

Besides the site projected density of states (PDOS), we discuss qualitatively the pair interactions based on the overlap population analysis with the crystal orbital overlap population (COOP) [51]. In the plots, positive, negative, and zero COOP magnitudes indicate bonding, anti-bonding, and non-bonding interactions, respectively.

Discussion

Crystal chemistry

Single crystals of the germanides $RE_2Nb_3Ge_4$ and $RE_2Ta_3Ge_4$ can be grown by repeated arc-melting of samples of the ideal starting compositions. These germanides crystallize with the orthorhombic $Ce_2Sc_3Si_4$ structure [10, 11], space group *Pnma*, a ternary ordered

Table 4. Atomic coordinates and isotropic displacement parameters (pm^2) for $RE_2Nb_3Ge_4$ (RE = Sc, Y, Gd–Er, Lu) and $Sc_2Ta_3Ge_4$. U_{eq} is defined as one third of the trace of the orthogonalized U_{ij} tensor.

Atom	Site	x	y	z	U_{eq}
$Sc_{2.04}Nb_{2.96}Ge_4$					
Sc*[a]	8*d*	–0.00721(6)	0.59410(2)	0.17666(4)	69(1)
Nb1	4*c*	0.16758(4)	1/4	0.49100(3)	46(1)
Nb2*[b]	8*d*	0.34267(3)	0.12583(1)	0.17102(2)	52(1)
Ge1	4*c*	0.30767(3)	1/4	0.85241(4)	57(1)
Ge2	4*c*	0.04233(5)	1/4	0.11183(4)	58(1)
Ge3	8*d*	0.18185(4)	0.04020(2)	0.46588(3)	64(1)
$Y_2Nb_3Ge_4$					
Y	8*d*	–0.0027(3)	0.5948(1)	0.1736(2)	221(3)
Nb1	4*c*	0.1647(4)	1/4	0.4887(3)	206(4)
Nb2	8*d*	0.3399(2)	0.1265(1)	0.1716(2)	216(3)
Ge1	4*c*	0.3046(4)	1/4	0.8630(3)	227(5)
Ge2	4*c*	0.0403(4)	1/4	0.1215(3)	216(5)
Ge3	8*d*	0.1739(3)	0.0416(1)	0.4610(2)	229(4)
$Gd_2Nb_3Ge_4$					
Gd	8*d*	–0.00202(5)	0.5950(1)	0.17268(4)	56(1)
Nb1	4*c*	0.1645(1)	1/4	0.48783(9)	46(2)
Nb2	8*d*	0.33924(8)	0.12668(4)	0.17171(7)	50(1)
Ge1	4*c*	0.3045(1)	1/4	0.8656(1)	52(2)
Ge2	4*c*	0.0392(1)	1/4	0.1232(1)	52(2)
Ge3	8*d*	0.1717(1)	0.04215(5)	0.46038(8)	57(1)
$Tb_2Nb_3Ge_4$					
Tb	8*d*	–0.00229(5)	0.5950(1)	0.17318(4)	89(1)
Nb1	4*c*	0.1649(1)	1/4	0.4885(1)	75(2)
Nb2	8*d*	0.3397(1)	0.12649(4)	0.17150(7)	75(1)
Ge1	4*c*	0.3047(1)	1/4	0.8638(1)	88(2)
Ge2	4*c*	0.0394(1)	1/4	0.1222(1)	83(2)
Ge3	8*d*	0.1727(1)	0.04194(6)	0.46101(8)	95(2)
$Dy_2Nb_3Ge_4$					
Dy	8*d*	–0.00229(2)	0.59498(1)	0.17350(2)	64(1)
Nb1	4*c*	0.16472(6)	1/4	0.48836(6)	52(1)
Nb2	8*d*	0.34009(4)	0.12659(2)	0.17172(4)	50(1)
Ge1	4*c*	0.30408(7)	1/4	0.86237(7)	66(1)
Ge2	4*c*	0.03969(7)	1/4	0.12068(7)	63(1)
Ge3	8*d*	0.17313(5)	0.04172(3)	0.46128(5)	73(1)
$Ho_2Nb_3Ge_4$					
Ho	8*d*	–0.00317(3)	0.59459(2)	0.17380(3)	61(1)
Nb1	4*c*	0.16531(8)	1/4	0.48879(7)	46(1)
Nb2	8*d*	0.34011(6)	0.12629(3)	0.17136(5)	50(1)
Ge1	4*c*	0.3048(1)	1/4	0.86105(9)	56(1)
Ge2	4*c*	0.0398(1)	1/4	0.12002(9)	54(1)
Ge3	8*d*	0.17453(7)	0.04141(4)	0.46157(7)	61(1)
$Er_2Nb_3Ge_4$					
Er	8*d*	–0.00363(5)	0.59456(2)	0.17409(4)	69(1)
Nb1	4*c*	0.1659(1)	1/4	0.4890(1)	51(2)
Nb2	8*d*	0.3404(1)	0.12615(5)	0.17130(9)	53(2)
Ge1	4*c*	0.3053(2)	1/4	0.8605(1)	63(3)
Ge2	4*c*	0.0405(2)	1/4	0.1195(2)	53(3)
Ge3	8*d*	0.1753(11)	0.04134(7)	0.4622(1)	65(2)
$Lu_2Nb_3Ge_4$					
Lu	8*d*	–0.00473(8)	0.59445(3)	0.17500(5)	63(1)
Nb1	4*c*	0.1663(2)	1/4	0.4894(2)	44(2)
Nb2	8*d*	0.3411(1)	0.12583(6)	0.1712(1)	34(1)
Ge1	4*c*	0.3060(2)	1/4	0.8585(2)	53(3)
Ge2	4*c*	0.0410(2)	1/4	0.1178(2)	47(3)
Ge3	8*d*	0.1769(2)	0.04126(8)	0.4632(1)	64(2)
$Sc_{2.19}Ta_{2.81}Ge_4$					
Sc*[c]	8*d*	–0.0094(1)	0.59415(6)	0.1764(1)	71(2)
Ta1	4*c*	0.16895(5)	1/4	0.49079(4)	47(1)
Ta2*[d]	8*d*	0.34398(3)	0.1260(1)	0.17081(3)	53(1)
Ge1	4*c*	0.3104(1)	1/4	0.8510(1)	56(2)
Ge2	4*c*	0.0439(1)	1/4	0.1118(1)	54(2)
Ge3	8*d*	0.18356(8)	0.04037(4)	0.46582(7)	63(1)

* These sites show mixed occupancies:
a) 0.942(2) Sc + 0.058(2) Nb
b) 0.924(2) Nb + 0.076(2) Sc
c) 0.977(2) Sc + 0.023(2) Ta
d) 0.884(2) Ta + 0.116(2) Sc

version of the Sm_5Ge_4 type [8, 9]. Only the two scandium compounds show Sc/Nb respectively Sc/Ta mixing. This could have been expected. Scandium is the smallest rare earth element and closer in size to niobium and tantalum. Nevertheless, small homogeneity ranges can be expected for all of these compounds.

Although the magnetic data of these niobium and tantalum compounds have been reported [28], a detailed crystal chemical discussion has not been performed, since precise single-crystal data were not available. In the following discussion we exemplarily focus on the structure of $Gd_2Nb_3Ge_4$.

The cation sites 8*d* (2×) and 4*c* are occupied in an ordered manner by gadolinium (8*d*), Nb1 (8*d*) and Nb2 (4*c*) atoms. In going from Gd_5Ge_4 [6] to $Gd_2Nb_3Ge_4$, we observe a drastic decrease of the lattice parameters: $a = 769.84$ pm → 700.98 pm, $b = 1483.72$ pm → 1353.6 pm, $c = 778.72$ pm → 717.87 pm. This is a direct consequence of the difference in the atomic radii [52] between gadolinium (180 pm) and niobium (125 pm). The shrinking of the unit cell has direct consequences on the metal coordination. While the three crystallographically independent gadolinium sites in Gd_5Ge_4 all have CN6 (299 – 325 pm for Gd1, 289 – 308 pm for Gd2 and 299 – 317 pm for Gd3), we observe differences in $Gd_2Nb_3Ge_4$. Nb1 (273 – 288 pm) and Nb2 (263 – 277 pm) still have CN6, but the gadolinium atoms have CN7 with Gd–Ge

Table 5. Interatomic distances (pm) of $Gd_2Nb_3Ge_4$ calculated with the powder lattice parameters. All distances within the first coordination spheres are listed. Standard deviations are all equal or less than 0.1 pm.

Gd:	1	Ge3	286.3	Nb2:	1	Ge2	263.0	Ge1:	1	Ge2	262.3
	1	Ge1	287.0		1	Ge3	264.3		1	Nb1	273.4
	1	Ge3	297.7		1	Ge2	270.8		2	Nb2	277.1
	1	Ge1	299.6		1	Ge3	274.4		2	Gd	287.0
	1	Ge2	299.7		1	Ge3	276.4		1	Nb1	288.4
	1	Ge3	303.2		1	Ge1	277.1		2	Gd	299.6
	1	Ge3	309.7		1	Nb1	304.9	Ge2:	1	Ge1	262.3
	1	Nb2	338.9		1	Nb1	307.2		2	Nb2	263.0
	1	Nb1	341.2		1	Nb2	333.9		2	Nb2	270.8
	1	Nb1	342.9		1	Gd	338.9		1	Nb1	274.5
	1	Nb2	344.7		1	Gd	344.7		1	Nb1	276.1
	1	Gd	357.2		2	Nb2	368.1		2	Gd	299.7
	2	Gd	367.7		1	Gd	378.4	Ge3:	1	Nb2	264.3
	1	Nb2	378.4		1	Gd	379.7		1	Ge3	272.4
	1	Nb2	379.7		1	Gd	383.7		1	Nb2	274.4
	1	Nb2	383.7						1	Nb2	276.4
	1	Gd	419.7						1	Nb1	282.1
Nb1:	1	Ge1	273.4						1	Gd	286.3
	1	Ge2	274.5						1	Gd	297.7
	1	Ge2	276.1						1	Gd	303.2
	2	Ge3	282.1						1	Gd	309.7
	1	Ge1	288.4								
	2	Nb2	304.9								
	2	Nb2	307.2								
	2	Gd	341.2								
	2	Gd	342.9								

Table 6. Calculated charges (Q) for Y_5Ge_4 and $Y_2Nb_3Ge_4$.

Compound	Y_5Ge_4	$Y_2Nb_3Ge_4$
Q(Y1)	+1.41	+1.42
Q(2)	+1.31(Y)	+0.57(Nb)
Q(3)	+1.32(Y)	+0.63(Nb)
Q(Ge1)	−1.59	−1.17
Q(Ge2)	−1.74	−1.03
Q(Ge3)	−1.71	−1.24

distances ranging from 286 to 310 pm. In view of these differences in coordination number, Gd_5Ge_4 and $Gd_2Nb_3Ge_4$ are, strictly speaking, rather isopointal [53, 54] than isotypic.

The Nb–Ge distances for the two crystallographically independent niobium atoms in $Gd_2Nb_3Ge_4$ range from 263 to 288 pm, slightly longer than the sum of the covalent radii of 256 pm [52]. Similar Nb–Ge distances have been observed in the A15 superconductor Nb_3Ge (287 pm) [55] and in $NbGe_2$ (269 – 290 pm) [56]. We can thus assume a considerable degree of covalent Nb–Ge bonding in $Gd_2Nb_3Ge_4$.

Fig. 1 gives a view of the $Gd_2Nb_3Ge_4$ structure approximately along the z axis. The Nb2 atoms lie on

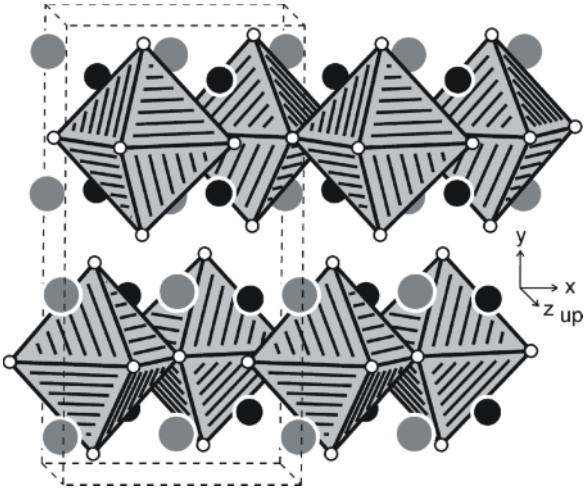

Fig. 1. View of the $RE_2Nb_3Ge_4$ structure approximately along the c axis. Rare earth, niobium and germanium atoms are drawn as medium grey, black filled and open circles, respectively. The network of corner-sharing $Nb2Ge_6$ octahedra is emphasized.

the mirror planes at $y = 1/4$ and $y = 3/4$ and have almost regular octahedral germanium coordination. These $Nb2Ge_6$ octahedra are condensed *via* common corners within the mirror planes (Fig. 2). In order to keep sufficient Nb–Ge bonding for these octahedra (as compared to Gd_5Ge_4), the unit cell is shrinking in b direction (*vide supra*). This further influences the Ge–Ge interactions. Ge_2 dumbbells and isolated atoms (*i. e.* no Ge–Ge bonding) in Gd_5Ge_4, but weak inter-layer Ge–Ge bonding (272 pm Ge3–Ge3) in $Gd_2Nb_3Ge_4$.

The connectivity of the two $NbGe_6$ and the $GdGe_7$ building units is shown in Fig. 2. The $Nb1Ge_6$ and $GdGe_7$ units are connected *via* common edges leading to strands that extend in x direction. Both of these strands condense with the network of $Nb2Ge_6$ octahedra *via* common faces, forming the densely packed structure.

Finally we draw back to the germanium substructures in Gd_5Ge_4 and $Gd_2Nb_3Ge_4$. To a first approximation one can consider the isolated Ge^{4-} units (no interlayer Ge–Ge bonding) and Ge_2^{6-} dumbbells (269 pm Ge–Ge) for the anionic part of the structure that is opposed to five Gd^{3+} cations. This would result in a Zintl-precise formulation $(5Gd^{3+})(2Ge^{4-})(Ge_2^{6-})\cdot e^-$. Considering that the Ge–Ge bonds are longer than in elemental germanium (245 pm) [57], the excess electron can also be counted at the germanium dumbbell, weakening its bond. Such a simple electron count is not

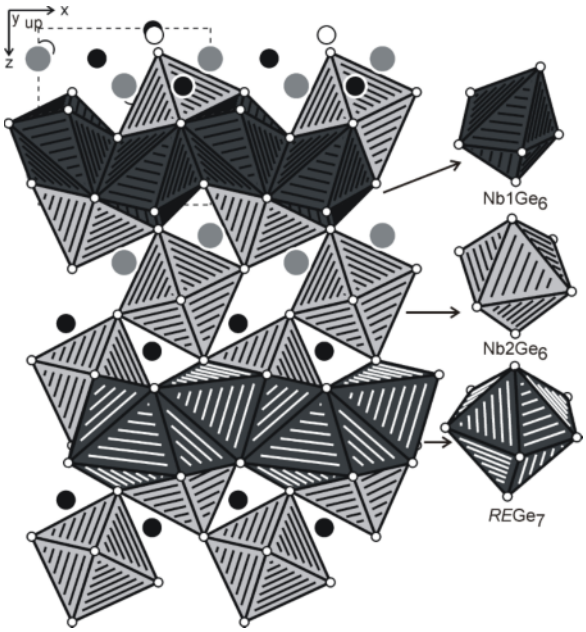

Fig. 2. Projection of the $RE_2Nb_3Ge_4$ structure along the b axis. Rare earth, niobium and germanium atoms are drawn as medium grey, black filled and open circles, respectively. The network of condensed metal-germanium polyhedra is emphasized. The three types of polyhedra are shown at the right-hand part in slightly different orientation.

possible for $Gd_2Nb_3Ge_4$: (i) the niobium atoms deliver more valence electrons and (ii) the inter-layer Ge–Ge distances become much shorter (272 pm). These differences in chemical bonding are addressed in more detail in the following paragraph using the crystallographic data of Y_5Ge_4 [6] and $Y_2Nb_3Ge_4$. The use of the yttrium compounds facilitates the electronic structure calculations (no f-electron contribution).

Electronic structure charge trends and chemical bonding

The site projected density of states PDOS is shown in Fig. 3. The energy reference along the x axis is with respect to the Fermi level (E_F). From their electronic configurations already at the atomic state, Y ({Kr}, $4d^1$, $5s^2$), the Y(d) PDOS is found centered above E_F within the (empty) conduction band. Below E_F within the valence band (VB) the similar PDOS shapes between the different constituents signal quantum mixing between the valence states, especially the itinerant part of Y(d) with Ge(p) in the energy windows –4 eV to E_F.

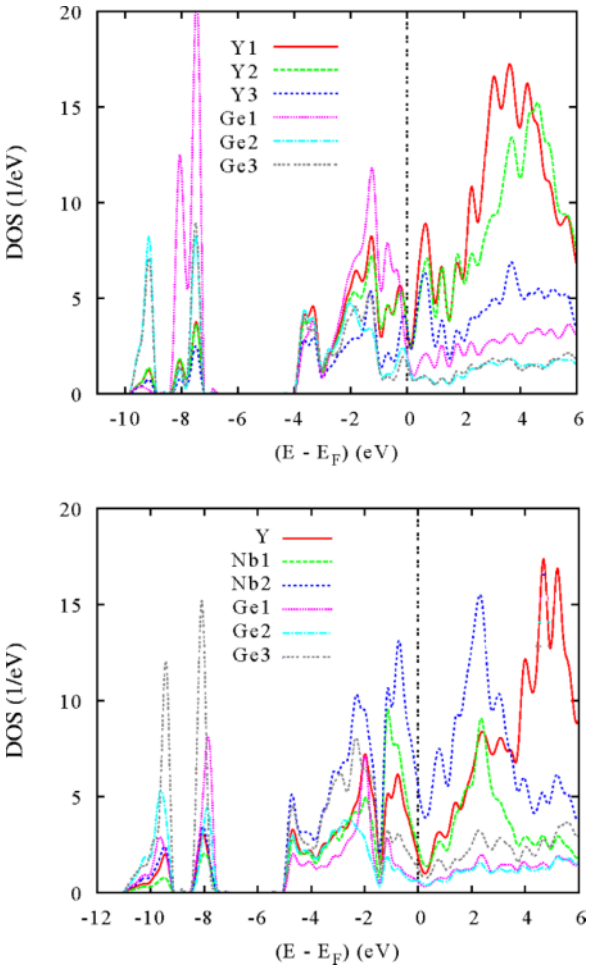

Fig. 3 (color online). Site projected density of states (PDOS) in Y_5Ge_4 (top) and $Y_2Nb_3Ge_4$ (bottom).

At lower energy, between −10 and −7 eV, less mixing between Y and Ge PDOS signals less s-like bonding at low energies (*cf.* Fig. 4). The lower panel illustrating the PDOS for the ternary compound shows differences due to the presence of Nb which brings two more electrons, Nb ({Kr}, $4d^4$, $5s^1$). The result is a broader and more structured PDOS zone extending 5 eV below the top of VB. E_F crosses larger PDOS arising from niobium (Nb2) whereas a deep minimum at E_F was observed for the binary compound. The lower part of the VB shows similar features as in the above panel but with less sharp and broader PDOS. These features point to a more covalently bonded ternary compound.

This is illustrated from the total COOP for the chemical bonding within the crystal studied comparatively

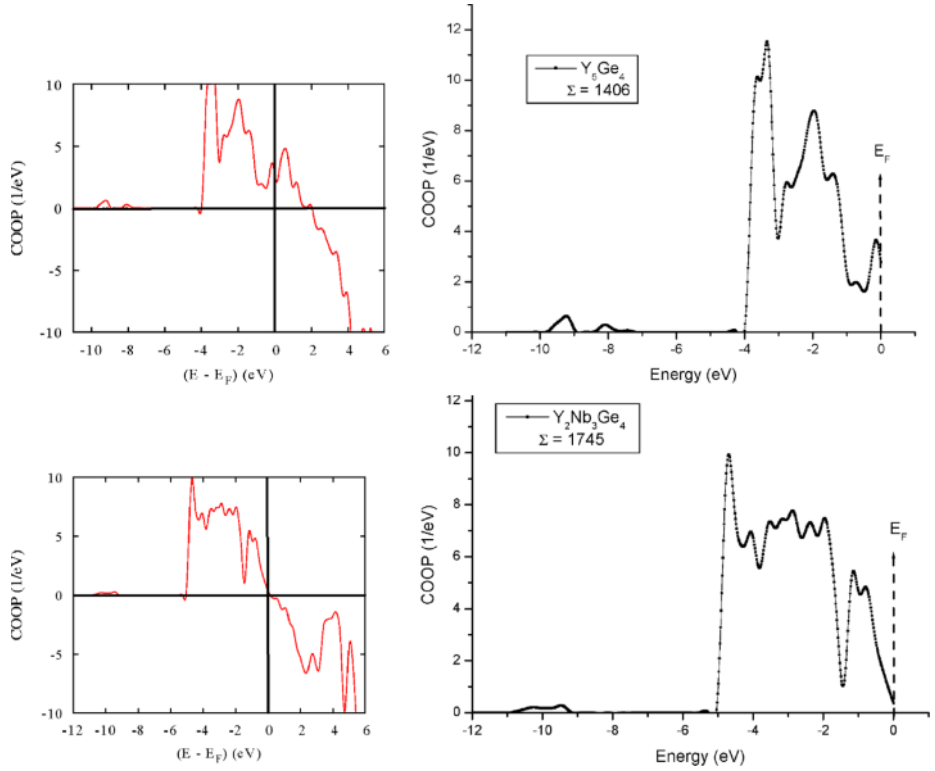

Fig. 4 (color online). Relative magnitudes of chemical bonding from TOTAL COOP in Y_5Ge_4 (top) and $Y_2Nb_3Ge_4$ (bottom). The panels at the right hand side show the VB bonding zone (below E_F) with Σ values indicating the statistics on the total COOP within VB, the bond strength being larger in the ternary compound.

for the two compounds in Fig. 4. As suggested by the DOS analysis, the bonding is mainly in the energy zone below E_F with the same extension as in the DOS, *i. e.* 4 eV in the binary compound and 5 eV in the ternary compound with larger intensity. The whole range of the VB is of bonding nature (positive COOP magnitudes). From visual inspection the bonding in the ternary compound is stronger. Since the bonding occurs where the electrons are, *i. e.* within the VB, we further quantify this observation by establishing statistics on the COOP intensities. On the right hand side panels, the COOPs are reproduced for the VB only. The inserts show the summations with the Σ values which are such that a stronger overall bonding can clearly be identified for $Y_2Nb_3Ge_4$.

These results can be further quantified by assessing the partial charges on each atomic constituent after self-consistent convergence. The analysis is based on Bader's 'Atom in Molecule' theory [58]. Typically in chemical systems, the charge density reaches a minimum between atoms, and this is a natural region to separate them from each other. Such an analysis does not constitute a tool for evaluating absolute ionizations but allows establishing trends between similar compounds. The values obtained for Y_5Ge_4 and $Y_2Nb_3Ge_4$ are listed in Table 6. The charge transfers are from Y to Ge in Y_5Ge_4 and from Y/Nb to Ge in $Y_2Nb_3Ge_4$. In the 'cationic' substructure the major effect is brought about by Nb which releases less charge due to its higher electronegativity ($\chi = 1.60$) with respect to Y ($\chi = 1.22$). Focusing on the germanium substructures, there is a lower charge transfer in $Y_2Nb_3Ge_4$. The charge analyses confirm the trend of stronger covalent bonding upon partial substitution of Y by Nb.

Acknowledgement

This work was supported by the Deutsche Forschungsgemeinschaft. We acknowledge computational facilities provided by the MCIA-Univ. Bordeaux clusters.

[1] V. K. Pecharsky, K. A. Gschneidner, Jr., *Phys. Rev. B* **1997**, *78*, 4494.
[2] V. K. Pecharsky, K. A. Gschneidner, Jr., *Appl. Phys. Lett.* **1997**, *70*, 3299.
[3] V. K. Pecharsky, K. A. Gschneidner, Jr., *Adv. Cryog. Eng.* **1998**, *43*, 1729.
[4] K. A. Gschneidner, Jr., V. K. Pecharsky, A. O. Tsokol, *Rep. Prog. Phys.* **2005**, *68*, 1479.
[5] G. J. Miller, *Chem. Soc. Rev.* **2006**, *35*, 799.
[6] S. Misra, G. J. Miller, *J. Am. Chem. Soc.* **2008**, *130*, 13900.
[7] V. Svitlyk, Y. Y. J. Cheung, Yu. Mozharivskyj, *J. Magn. Magn. Mater.* **2010**, *322*, 2558.
[8] G. S. Smith, A. G. Tharp, Q. Johnson, *Nature* **1966**, *210*, 1148.
[9] G. S. Smith, Q. Johnson, A. G. Tharp, *Acta Crystallogr.* **1967**, *22*, 269.
[10] I. R. Mokraya, O. I. Bodak, E. I. Gladyshevskii, *Sov. Phys. Crystallogr.* **1979**, *24*, 729.
[11] O. I. Bodak, V. K. Pecharskii, Ya. M. Kalychak, O. I. Kharchenko, I. R. Mokra, L. O. Muratova, D. A. Beryezyuk, M. M. Shyevchuk, *Fazovye Ravnovesiya Met. Splavakh* **1981**, 57.
[12] Z. M. Shpyrka, V. A. Bruskov, I. R. Mokraya, V. K. Pecharskii, O. I. Bodak, P. Yu. Zavalii, *Izv. Akad. Nauk Ukr. SSSR, Neorg. Mater.* **1990**, *26*, 969.
[13] B. Ya. Kotur, I. R. Mokra, A.Ya. Toporinskii, *Izv. Akad. Nauk Ukr. SSSR, Metally* **1991**, 204.
[14] B. Ya. Kotur, O. E. Banakh, R. Černý, J. V. Pacheco Espejel, *J. Alloys Compd.* **1997**, *260*, 157.
[15] O. E. Banakh, B. Ya. Kotur, *J. Alloys Compd.* **1998**, *268*, L3.
[16] A. V. Morozkin, Yu. D. Seropegin, V. K. Portnoy, A. V. Leonov, I. A. Sviridov, *J. Alloys Compd.* **1998**, *281*, L1.
[17] H. Flandorfer, J. Gröbner, A. Kostikas, C. Godart, P. Rogl, V. Psicharis, A. Saccone, R. Ferro, G. Effenberg, *J. Alloys Compd.* **2000**, *297*, 129.
[18] A. V. Morozkin, R. Welter, *J. Alloys Compd.* **2002**, *336*, 202.
[19] A. V. Morozkin, *J. Alloys Compd.* **2004**, *377*, L4.
[20] U.Ch. Rodewald, B. Heying, D. Johrendt, R.-D. Hoffmann, R. Pöttgen, *Z. Naturforsch.* **2004**, *59b*, 174.
[21] S. Misra, G. J. Miller, *Acta Crystallogr. E* **2009**, *65*, i25.
[22] A. V. Morozkin, Yu.D. Seropegin, V. K. Portnoy, A. V. Leonov, I. A. Sviridov, *J. Alloys Compd.* **1998**, *278*, L8.
[23] A. V. Morozkin, Yu.D. Seropegin, I. A. Sviridov, V. A. Moskalev, *J. Alloys Compd.* **1998**, *281*, 228.
[24] A. V. Morozkin, *J. Alloys Compd.* **1999**, *287*, 185.
[25] B. Ya. Kotur, *Dopov. Akad. Nauk Ukr. RSR (Ser. A)* **1986**, 82.
[26] Yu. D. Seropegin, M. V. Rudometkina, *J. Less-Common Met.* **1987**, *135*, 127.
[27] T. Le Bihan, H. Noël, P. Rogl, *J. Alloys Compd.* **1994**, *213/214*, 540.
[28] T. Le Bihan, K. Hiebl, P. Rogl, H. Noël, *J. Alloys Compd.* **1995**, *235*, 80.
[29] K. W. Richter, H. F. Franzen, *J. Solid State Chem.* **2000**, *150*, 347.
[30] T. Lebihan, P. Rogl, H. Noël, *J. Nucl. Mater.* **2000**, *277*, 82.
[31] P. Warczok, F. Mittendorfer, G. Kresse, A. Kroupa, H. Ipser, K. W. Richter, *Solid State Sci.* **2007**, *9*, 159.
[32] M. Sikiritsa, O. I. Bodak, B. Ya. Kotur, *Tezizy Dokl. Vses. Konf. Kristallokhim. Intermet. Soeden. (4th)* **1983**, 76.
[33] Yu. O. Seropegin, V. V. Tabachenko, M. G. Mys'kiv, *Kristallografiya* **1984**, *29*, 161.
[34] B. Ya. Kotur, O. I. Bodak, V. E. Zavodnik, *Kristallografiya* **1986**, *31*, 868.
[35] B. Ya. Kotur, O. I. Bodak, *Izv. Akad. Nauk Ukr. SSSR, Metally* **1988**, 189.
[36] B. Ya. Kotur, O. M. Boznyak, O. I. Bodak, *Izv. Akad. Nauk SSSR, Neorg. Mater.* **1989**, *25*, 399.
[37] B. Ya. Kotur, O. I. Bodak, *Izv. Akad. Nauk Ukr. SSSR, Metally* **1990**, 200.
[38] M. Song, S. Mao, J. X. Mi, J. Zhao, *Xiamen Daxue Xuebao (Ziran Kexueban)* **1999**, *38*, 225.
[39] B. Reker, D. Johrendt, R. Pöttgen, *Intermetallics* **2013**, *38*, 36.
[40] R. Pöttgen, Th. Gulden, A. Simon, *GIT Labor-Fachzeitschrift* **1999**, *43*, 133.
[41] K. Yvon, W. Jeitschko, E. Parthé, *J. Appl. Crystallogr.* **1977**, *10*, 73.
[42] V. Petříček, M. Dušek, L. Palatinus, JANA2006, The Crystallographic Computing System, Institute of Physics, University of Prague, Prague (Czech Republic) **2006**.
[43] L. Palatinus, G. Chapuis, *J. Appl. Crystallogr.* **2007**, *40*, 786.
[44] G. M. Sheldrick, SHELXL-97, Program for the Refinement of Crystal Structures, University of Göttingen, Göttingen (Germany) **1997**.
[45] G. M. Sheldrick, *Acta Crystallogr.* **2008**, *A64*, 112.
[46] A. R. Williams, J. Kübler, C. D. Gelatt, Jr., *Phys. Rev. B* **1979**, *19*, 6094.
[47] V. Eyert, *The Augmented Spherical Wave Method – A Comprehensive Treatment*, Lecture Notes in Physics, Springer, Heidelberg, **2007**.
[48] P. Hohenberg, W. Kohn, *Phys. Rev.* **1964**, *136*, B864.
[49] W. Kohn, L. J. Sham, *Phys. Rev.* **1965**, *140*, A1133.
[50] J. Perdew, K. Burke, M. Ernzerhof, *Phys. Rev. Lett.* **1996**, *77*, 3865.
[51] R. Hoffmann, *Angew. Chem., Int. Ed. Engl.* **1987**, *26*, 846.

[52] J. Emsley, *The Elements*, Oxford University Press, Oxford **1999**.
[53] L. M. Gelato, E. Parthé, *J. Appl. Crystallogr.* **1987**, *20*, 139.
[54] E. Parthé, L. M. Gelato, *Acta Crystallogr.* **1984**, *A40*, 169.
[55] H. Holleck, F. Benesovsky, H. Nowotny, *Monatsh. Chem.* **1962**, *93*, 996.
[56] R. Kubiak, R. Horyn, H. Broda, K. Lukaszewicz, *Bull. Acad. Pol. Sci. (Ser. Sci. Chim.)* **1972**, *20*, 429.
[57] J. Donohue, *The Structures of the Elements*, Wiley, New York **1974**.
[58] R. F. W. Bader, *Chem. Rev.* **1991**, *91*, 893.